Chinese Chemical Letters 34 (2023) 107535

Contents lists available at ScienceDirect

Chinese Chemical Letters

journal homepage: www.elsevier.com/locate/cclet

Developing high-quality g-C_3N_4 film electrode for the photoelectrocatalytic degradation of methylene blue in water

Yanxi Gong[a], Jianbing Wang[a,*], Zikun Cheng[a], Zhiyuan Han[a], Xu Zhao[b], Buyu Chai[a], Yuanchun Han[a]

[a] China University of Mining and Technology-Beijing, Beijing 100083,China
[b] Research Center for Eco-Environment Sciences, Chinese Academy of Sciences, Beijing 100085,China

ARTICLE INFO

Article history:
Received 17 December 2021
Revised 25 March 2022
Accepted 14 May 2022
Available online 19 May 2022

Keywords:
Graphitic carbon nitride
Photoelectrochemical activity
Methylene blue
Degradation pathway
Synergistic effect

ABSTRACT

Developing a high-quality photoelectrode for photoelectrochemical applications is still an ongoing challenge. In this study, we prepared the g-C_3N_4 film on the indium tin oxide (ITO) glass through conventional coating, liquid-based growth, *in-situ* calcination, and vapor deposition methods, respectively. These electrodes were characterized and used as photoanodes to degrade methylene blue (MB) in water. Among these methods, the *in-situ* calcination method was most appropriate for preparing the continuous and organized g-C_3N_4 film electrodes with uniform g-C_3N_4 coverage and strong adhesion to the ITO substrate. It also had the highest activity in the photocatalytic (PC), electrochemical (EC), and photoelectrocatalytic (PEC) degradation processes of MB. In the PEC reaction, at an applied potential of 1.0 V and a light intensity of 0.96 W/cm^2, the removal rate of MB was 62.5%, which was much higher than those in the PC and EC reactions. The high degradation rate was due to the synergistic effect of PEC degradation, wherein the PC and EC reactions promote and optimize each other. In the PC reaction, MB was degraded by $-CH_3$ elimination, while the EC degradation pathway mainly included the conversion of sulfhydryl into sulfoxide and the opening of the central aromatic ring. Both methyl loss and aromatic ring opening occurred in the PEC reaction. Moreover, some monocyclic compounds were formed, and MB showed more complete degradation in the PEC reaction.

In the past decades, photocatalysis using semiconductors had garnered considerable attention owing to its potential to degrade recalcitrant organic compounds in water [1,2]. TiO_2 had been extensively studied among various semiconductors because of its non-toxicity, good stability, and excellent catalytic activity [3]. However, TiO_2 was not an optimal photocatalyst capable of utilizing visible light because of its wide bandgap (3.2 eV) [4].

A polymer-like semiconductor material (g-C_3N_4) might be a promising photocatalyst owing to a bandgap of 2.7 eV and visible light photocatalytic (PC) activity [5–8]. Such materials were also free of metals, easily prepared, inexpensive, environmentally benign, and stale in a corrosive chemical environment. Such superior properties resulted in the extensive study of the application of g-C_3N_4 in the PC degradation of organic pollutants [9]. Bulk g-C_3N_4 could be prepared by a straightforward polymerization method involving the thermal condensation of nitrogen- and carbon-rich monomers such as dicyanamide, melamine, and cyanamide [10,11]. Researchers used various approaches to improve the PC properties of g-C_3N_4, including doping [12–15], semiconductor recombination [16,17], supermolecular assembly [18], the introduction of pores by templating methods [11,19], and surface heterojunction design [20,21]. A direct and continuous g-C_3N_4 layer was preferred for the PC degradation of organic compounds in water; g-C_3N_4 was usually loaded on substrates (*e.g.*, non-conductive substrates such as aluminum oxide and conductive transparent oxides such as fluorine doped tin oxide (FTO) and indium tin oxide (ITO)) for use [22,23]. To improve the performance of the g-C_3N_4 film on the substrate, researchers designed heterostructures comprising g-C_3N_4 and metal oxides such as ZnO to enhance the PC activity [24]. Additionally, modified ITO substrates such as photonic crystal fluorine-doped tin oxide (PC-FTO) were used to increase the overall photon-electron conversion efficiency under illumination [25].

Despite the progress in the synthetic routes of g-C_3N_4, the PC activity of the g-C_3N_4 film was limited due to the strong recombination of charge carriers [26]. Recently, a study showed that g-C_3N_4 films supported on the ITO glass by a dip coating method could achieve the combination of PC and electrochemical (EC) oxi-

* Corresponding author.
E-mail address: wangjb@cumtb.edu.cn (J. Wang).

https://doi.org/10.1016/j.cclet.2022.05.049
1001-8417/

dation, resulting in photoelectrocatalytic (PEC) oxidation [27]. Owing to the water-insoluble nature and large particles of g-C_3N_4, the general deposition methods (spin coating and screen printing) resulted in poor g-C_3N_4 coverage and weak adhesion on the conductive transparent substrates such as FTO and ITO [28]. Thus, the dip coating method resulted in only a minimal amount of g-C_3N_4 being firmly attached to the ITO glass, and the resultant g-C_3N_4 films often exhibited low conductivity and showed unsatisfying activity in water treatment. Another report described the preparation and use of a nonstoichiometric titanium oxide electrode for the PEC degradation of bisphenol A in water [29]; however, the electrode was not apparent and did not allow light transmission. Additionally, the preparation process was rather complex and the reduction step used hydrogen gas, which was dangerous. Therefore, more detailed investigations are required to develop a method for the easy fabrication of high-quality g-C_3N_4 film electrodes. Moreover, a detailed understanding of the PEC process with the g-C_3N_4 film electrode was still lacking. Further research was required to thoroughly understand the mechanism of the PEC reaction.

Herein a g-C_3N_4 thin film was prepared on the ITO substrate using various methods. The resultant g-C_3N_4 film electrodes were characterized and studied for their electrochemical and photocatalytic activity as photoanodes in a PEC system to degrade methylene blue (MB) in water. Additionally, the intermediates produced from the PC, EC, and PEC reactions were identified to examine the MB degradation pathway and understand the synergy of PC and EC in the PEC reaction.

In this study, analytical-grade cyanuric acid, benzoguanamine, and melamine were purchased from a Japan chemical plant in Tokyo. Analytical-grade MB was purchased from Sinopharm Chemical Reagent Co., Ltd. Chromatographic-grade methanol was purchased from Beijing Dikma Technology Co., Ltd. The other analytical-grade chemicals were purchased from Beijing Blue Yi Chemical Products Co., Ltd. All solutions were prepared with deionized water from a Thermo Milli-Q Reagent Water System.

Conductive ITO glasses were purchased from Head (Beijing) Biotechnology Co., Ltd. Before use, they were washed with detergent to remove the pollutants on the surface and boiled with ammonia water, hydrogen peroxide, and water for 30 min. Subsequently, the ITO glasses were sonicated in ethanol for 15 min and finally preserved in ethanol.

Four methods were used to load g-C_3N_4 on the ITO glass, including *in-situ* calcination, vapor deposition, dip coating, and liquid-based growth method. The resultant g-C_3N_4 film electrodes were marked as I/g-C_3N_4, V/g-C_3N_4, D/g-C_3N_4, and L/g-C_3N_4 electrodes, respectively. The dip coating and liquid-based growth methods were based on the literature [27,30], and the procedures were stated in texts S1 and S2 (Supporting information).

For the *in-situ* calcination method, cyanuric acid and benzoguanamine with a molar ratio of 1:1 were mixed in 40 mL of deionized water. After stirring for 6 h, the mixture was centrifuged, and the white slurry was obtained after the supernatant was removed. A certain amount of white slurry was evenly coated on the ITO substrate, which was put in a quartz boat. The quartz boat was then dried, sealed with aluminum foil, and calcined for 3 h under the protection of nitrogen flow at a temperature of 450–550 °C. Before use, the I/g-C_3N_4 film electrode was treated by ultrasonic cleaning for 1 h to remove the residual aggregates on the surface.

Concerning the vapor deposition method, the electrode was prepared by a two-step process. In the first step, melamine was put into a capped aluminum oxide crucible and heated to 550 °C at a rate of 2 °C/min. After 4 h of calcination, a block of g-C_3N_4 was obtained. It was subsequently ground into powder. In the second step, 1 g of g-C_3N_4 powder was evenly spread in the quartz boat and covered by an ITO glass. Subsequently, a quartz glass plate was set on the top of the quartz boat to control as much steam in the quartz boat as possible. The quartz boat was heated to 500 °C at a rate of 2 °C/min and calcined for 3 h. Before use, the V/g-C_3N_4 film electrode was also treated by ultrasonic cleaning for 1 h to remove the residual aggregates on the surface.

X-ray diffraction (XRD) patterns were characterized using a PRO MPD X-ray diffractometer (PAN analytical, Netherlands) with Cu Kα radiation. The test voltage and current of XRD were 35 kV and 25 mA, respectively. The X-ray wavelength was 0.15418 nm, and the scanning angle was 5°−80°. The scanning speed was 10°/min.

Scanning electron microscopy (SEM) images were obtained on a Hitachi S450 scanning electron microscope (Hitachi, Japan). The morphology of g-C_3N_4 film electrodes was examined by Hitachi S450 SEM at an accelerating voltage of 10 kV. The Brunauer-Emmett-Teller (BET) surface area measurements were conducted on an ASAP 2010 HD88 nitrogen adsorption apparatus (Micromeritics Instruments, USA). Before the BET test, all samples were degassed at 120 °C for 12 h to completely remove the adsorbates from the samples. The nitrogen adsorption-desorption isotherms were measured at 77 K after degassing the samples. N_2 adsorption-desorption isotherms were measured on a physical absorber. The Fourier transform infrared (FTIR) spectra were analyzed on a Perkin Elmer System 2000 spectrometer (PerkinElmer, USA), at a frequency range of 4000–600 cm^{-1} with a resolution of 1 cm^{-1}. The diffuse reflectance spectroscopy (DRS) was recorded on a Hitachi U-3010 UV–vis spectrophotometer (Hitachi, Japan) using $BaSO_4$ as the reference. The detection wavelength range was 200–800 nm.

The MB concentration in an aqueous solution was analyzed using a Hitachi 3010 UV–vis spectrophotometer (Hitachi, Japan), and the maximum absorption wavelength was 664 nm.

The PC, EC, and PEC measurements were conducted using a CHI 660 B electrochemical workstation (Shanghai Chenhua Instrument Co., Ltd., China), a conventional three-electrode cell system connected with a counter electrode (Pt wire, with a length and diameter of 60 mm and 0.5 mm, respectively), a working electrode (the g-C_3N_4 film; active area of 8 cm^2), and a reference electrode (a saturated calomel electrode, SCE). Visible irradiation was obtained from a 500 W xenon lamp (Institute for Electric Light Sources, Beijing) with a 420 nm cutoff filter. The degradation experiments were conducted in a rectangular (50 mm × 50 mm × 60 mm) reactor made of quartz glass, containing an aqueous solution of MB (10 mg/L) and Na_2SO_4 electrolyte solution (0.05 mol/L).

The PC and EC experiments were conducted after turning off the electricity source and xenon lamp, respectively. The PEC experiments were conducted after simultaneously turning on the electricity source and xenon lamp.

We conducted a dark test to study the adsorption of MB on the g-C_3N_4 thin film electrode. 120 mL of a 10 mg/L MB solution was stirred at 250 r/min without the electrochemical workstation and the xenon lamp source. The reactor was wrapped by the foil to ensure complete darkness.

The intensity of the xenon lamp was tested every week throughout the experiment, and was stably maintained at about 0.96 W/cm^2 with a current of 15 A.

In the study, water samples were collected at different time periods to analyze the MB concentration and identify the degradation intermediates. Before the analysis, the water samples were filtered with a 0.22 μm polyethersulfone button membrane. The concentration of MB was determined by ultraviolet spectrophotometry.

The intermediate products of PC, EC and PEC oxidation of MB were identified by high-performance liquid chromatography-mass spectrometry (HPLC-MS), and compared using their total ion chromatograms (TIC). Electrospray ionization (ESI) was used as the ion source for HPLC-MS (Shimadzu LCMS 8040, Japan), and the liquid chromatography column was C8 (S/N 60,423,719, Japan). The mobile phase comprised a 0.1% formic acid solution and methanol with a ratio of 80%:20%, at a flow rate of 0.4 mL/min. The column

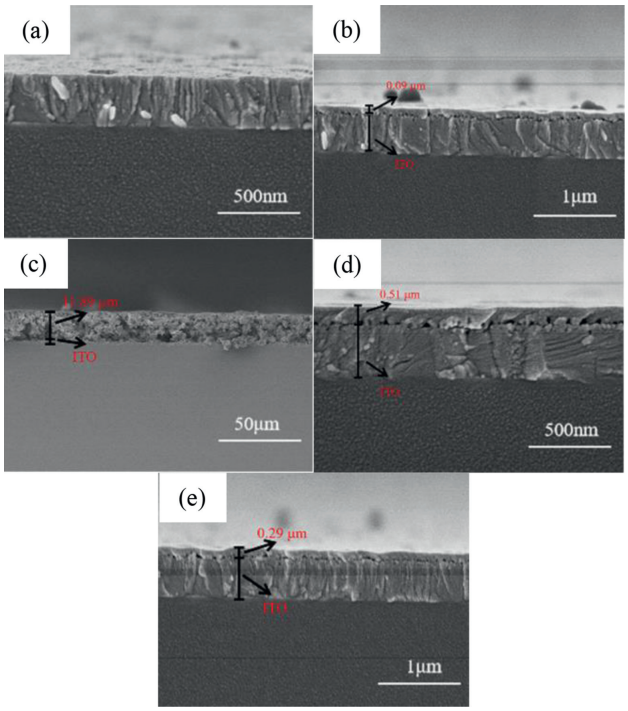

Fig. 1. SEM images of the (a) cross-section of the ITO substrate, (b) D/g-C_3N_4 film electrode, (c) L/g-C_3N_4 film electrode, (d) I/g-C_3N_4 film electrode, and (e) V/g-C_3N_4 film electrode at 500 °C.

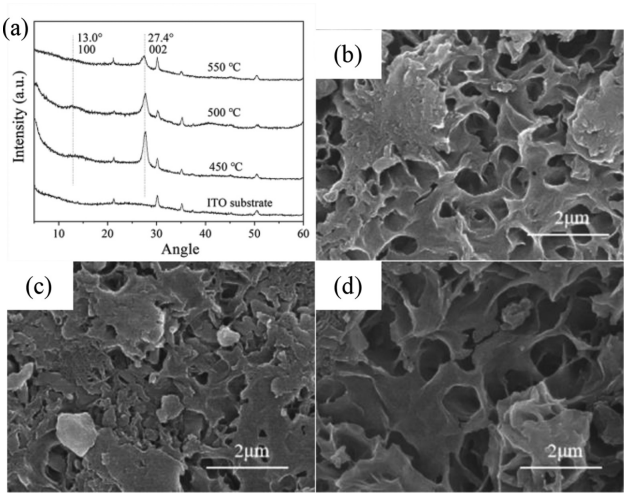

Fig. 2. (a) XRD patterns of I/g-C_3N_4 film electrodes at various temperatures and ITO glass substrates. The SEM images of I/g-C_3N_4 film electrodes calcined at (b) 450, (c) 500, and (d) 550 °C.

temperature was set as 30 °C. The scanning range was *m/z* 100–700 with positive and negative ions. The detected intermediates were analyzed using the product ion scanning (PIS) mode with a voltage of 25 V and a scanning range of *m/z* 50–600.

It was challenging to prepare high-quality g-C_3N_4 film electrodes with the characteristics of continuous and organized g-C_3N_4 strands, uniform g-C_3N_4 coverage, and strong adhesion to ITO glass [30]. Moreover, the thickness of the film should be moderate to facilitate the PEC reaction. The particle load was increased to the highest extent to ensure that the film was transparent, and to provide as many active sites as possible.

Fig. 1 shows SEM images of the cross-section of the ITO glass and various electrodes. The ITO glass was transparent and the ITO thickness was about 300 nm (Fig. 1a). The thickness of the g-C_3N_4 film on the D/g-C_3N_4 electrode was about 90 nm, which was much thinner than that of the ITO coating on the glass (Fig. 1b). The considerably thin film was mainly attributed to the absence of a calcination step in the dip-coating method. The calcination step was critical for producing strong adhesion between the g-C_3N_4 particles and ITO substrate. Without this step, only few g-C_3N_4 particles were firmly attached to the ITO glass. Therefore, the D/g-C_3N_4 film electrode usually possessed a considerably low loading of g-C_3N_4 on the ITO substrate, resulting in few active sites for the PC and EC oxidation and low activity of the PC, EC, and PEC reactions.

The thickness of the g-C_3N_4 film on the L/g-C_3N_4 electrode was as large as 11.89 μm (Fig. 1c), and was unfavorable for visible light transmission. In the liquid-growth method, the mixture of cyanuric acid (C) and 2,4-diamino-6-phenyl-1,3,5-triazine (Mp) in water was initially prepared. Subsequently, the dried CMp was directly loaded onto the ITO substrate. The electrode prepared by this method was marked as the L/g-C_3N_4 film electrode. With the calcination step, g-C_3N_4 could grow directly on the ITO glass to a thickness of up to >10 μm because of surface wettability [30]. Moreover, owing to the low conductivity of g-C_3N_4, the increase in the film thickness would decrease the electrochemical performance of the electrode. Additionally, this method usually resulted in an uneven distribution of the g-C_3N_4 particles on the ITO glass.

The g-C_3N_4 film on the I/g-C_3N_4 electrode had a suitable thickness of 0.51 μm (Fig. 1d). Moreover, the film was continuous and uniform. In the *in-situ* calcination method, the wet Mp mixture was initially coated onto the ITO glass. The powder could be attached to the ITO substrate more tightly due to surface wettability, and the g-C_3N_4 particles could grow directly on the ITO glass with the calcination step according to a principle similar to that of the liquid growth method. By optimizing the amount of the wet slurry, the film thickness could be controlled at a moderate level.

The thickness of the g-C_3N_4 film on the V/g-C_3N_4 electrode was about 0.29 μm (Fig. 1e). However, the g-C_3N_4 particles were unevenly distributed on the surface of the ITO glass. In this method, g-C_3N_4 was initially gasified and subsequently deposited on the ITO. Controlling the amount of g-C_3N_4 gas in the quartz boat was difficult as the nitrogen gas flow rate was unstable, thus making it hard to control the film thickness. Moreover, uneven deposition could easily occur in the quartz boat, resulting in a discontinuous membrane. All of these setbacks would lead to the poor performance of the prepared film electrode.

Fig. 2a shows the XRD patterns for the ITO glass substrate and I/g-C_3N_4 film electrode treated at a different temperature, respectively. For the film samples, the diffraction peaks at $2\theta = 13.0°$ were indexed as (100) in JCPDS No. 87-1526. The peaks were very weak, presumably because of the low amount of g-C_3N_4 on the ITO substrate. The calculated interplanar distance of the aromatic series is $d = 0.680$ nm, which is slightly smaller than the size of the tris-*s*-triazine unit (*ca.* 0.73 nm), perhaps due to the presence of the small tilt angularity in the structure [31]. The diffraction peak at 2θ of 27.4° is characteristic of interlayer stacking of the aromatic series, indexed as (002) diffraction for graphitic materials. The calculated interplanar distance of the aromatic series is $d = 0.324$ nm, which is in good agreement with previous studies [32]. Comparing to the I/g-C_3N_4 film electrodes calcined at different temperatures, the g-C_3N_4 electrode calcined at 450 °C had the most substantial peak at 2θ of 27.4°

Figs. 2b–d show the SEM images of I/g-C_3N_4 film electrodes obtained at different temperatures. These films have a porous structure and are made by the sheet-like structure superposition of different sizes. A slight difference exists in the pore size between various samples. The I/g-C_3N_4 film electrodes calcined at higher temperatures possessed a larger pore size, which may increase the

surface area and also the adsorption capacity of the I/g-C_3N_4 film electrodes [33].

Fig. S3 (Supporting information) shows the N_2 adsorption-desorption isotherms, and the corresponding pore size distribution curves of the powders scraped from the I/g-C_3N_4 film electrodes prepared at different calcination temperatures. All isotherms are of type IV (International Union of Pure and Applied Chemistry (IUPAC) classification) [13,34], indicating the presence of mesopores (2–50 nm). The hysteresis loops are associated with the silt-shaped pores resulting from the aggregates of plate-like particles [35]. The pore size distributions of the three samples show a wide range of 2–100 nm, with peak pore diameters of ~58, ~68, and ~72 nm at calcination temperatures of 500, 450, and 550 °C, respectively.

Strong absorption bands located at 1200–1650 cm^{-1} (Fig. S4a in Supporting information) are attributed to the typical stretching modes of C–N heterocycles [36]. The peak at 807 cm^{-1} can be assigned to the characteristic vibration of triazine units. A broad band ranging from 2900 cm^{-1} to 3200 cm^{-1} may be associated with the stretching vibration of N–H groups. An insignificant difference is observed between the FTIR spectra of I/g-C_3N_4 film electrodes prepared at different calcination temperatures.

The calculated bandgap based on the UV–vis diffuse reflectance spectra of the I/g-C_3N_4 film electrodes (Fig. S4b in Supporting information) is 2.39, 2.48, and 2.70 eV for calcination temperatures of 550, 500, and 450 °C, respectively [37]. Red-shift occurs with the increase in calcination temperature. This may be attributed to the effect of the large particle size of the I/g-C_3N_4 samples.

Fig. S4c (Supporting information) shows the transient photocurrent density responses of the I/g-C_3N_4 film electrodes under visible light irradiation ($\lambda > 420$ nm, $[Na_2SO_4] = 0.05$ mol/L). We observed that g-C_3N_4 has a rapid response to light. The photocurrent increased rapidly once the light was turned on. The electrodes were prepared at 500 °C and the photocurrent value reached a maximum of 3.1 μA, which is 1.38 and 2.48 times those of electrodes prepared at 450 °C (2.25 μA) and 550 °C (1.25 μA), respectively. This indicates that the electrode prepared at a calcination temperature of 500 °C may possess the best photoelectric performance, and can effectively improve the separation efficiency and migration rate of the photogenerated electrons and holes produced in g-C_3N_4.

Before testing the activity of various electrodes in the PC, EC, and PEC reactions, we conducted the adsorption and photolytic degradation experiments, and the results are shown in Fig. S6 (Supporting information). In the dark reactor without irradiation and electric current, the removal rate of MB after 2 h was no more than 0.5% for various electrodes. This indicated the negligible adsorption of MB on various g-C_3N_4 film electrodes. The degradation of MB was about 8.69% after 2 h of visible radiation in the absence of the g-C_3N_4 film electrode. Thus, we deduced that photolytic degradation has little effect on the removal of MB.

Fig. 3a shows the removal of MB after 2 h of reaction for the PC, EC, and PEC systems using various electrodes. In the PC reaction, about 25.08%–11.56% of MB was removed from the water using the three electrodes, indicating that the g-C_3N_4 film on ITO has low PC activity. When g-C_3N_4 was irradiated, photogenerated electrons and holes were generated from its conduction and valence bands, respectively. The photogenerated electrons and holes were then separated, and the g-C_3N_4 film had a certain PC activity as the photogenerated electrons could produce radicals to indirectly degrade the MB, and the photogenerated holes could be transmitted to the surface to directly oxidize MB [38]. The PC activity of the g-C_3N_4 film was low due to its high photoelectron-hole recombination rate [26].

The removal rates of MB in the EC oxidation experiments with an applied potential of 1 V were 21.70%–13.24% for the three types of electrodes. This indicated the EC activity of the g-C_3N_4 film on ITO; however, its catalytic efficiency was low. The EC activity of the g-C_3N_4 film on ITO was also reported in the previous literature [27]. The limited EC activity of the g-C_3N_4 film electrodes was mainly attributed to the low electrical conductivity of g-C_3N_4 [39].

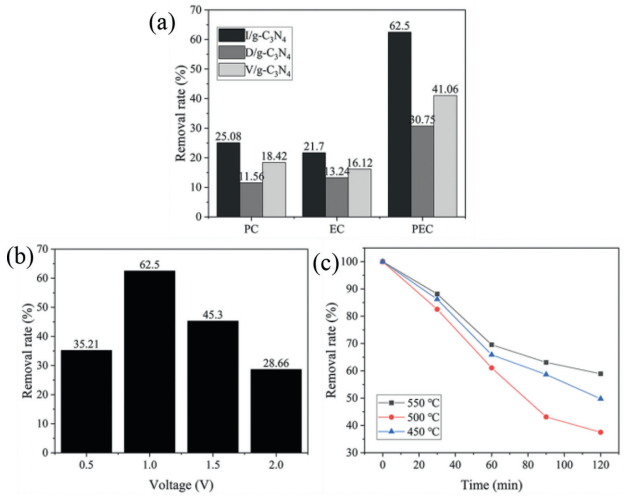

Fig. 3. (a) Removal rates of MB after 2 h of reaction in the PC, EC and PEC systems using various electrodes. (b) The removal rates of MB in the PEC reaction using the I/g-C_3N_4 film electrode at various potentials. (c) The removal rates of MB in the PEC reaction using the I/g-C_3N_4 film electrode prepared at different calcination temperatures.

At a potential of 1 V and light intensity of 0.96 W/cm^2, the removal rates of MB ranged from 62.50% to 30.75% after 2 h of reaction using the three electrode types (Fig. 3a). The removal rates of MB in all the PEC reactions using the three kinds of electrodes were much higher than those in the PC and EC reactions. The total organic carbon (TOC) values of the solution samples withdrawn before and after the reaction with the I/g-C_3N_4 film electrode were also measured and the results are shown in Fig. S7 (Supporting information). Notably, the removal rate of TOC was not very high in the PEC process (about 24.1%). However, the removal rate of TOC in the PEC process was much higher than those in the PC and EC reactions.

This indicates the enhancement of MB degradation through PEC using these electrodes. According to the literature [27], the synergistic effect of PEC degradation was proposed to explain the dramatic enhancement of degradation in the previous study. The visible light irradiation promoted the EC oxidation as it eliminated electrode passivation through the photogenerated electrons and holes at low potentials and produce an active oxidation agent to enhance the EC oxidation of MB. Simultaneously, the applied bias could reduce the recombination of the photogenerated electrons and holes, and improve the separation of photogenerated charge carriers and promote the PC oxidation of MB.

Fig. 3a also shows that the I/g-C_3N_4 film electrode is more active in the PC, EC, and PEC reactions compared to the V/g-C_3N_4 and D/g-C_3N_4 film electrodes. Its excellent performance resulted from the high quality of the I/g-C_3N_4 film electrode mentioned above. This further proves that the *in-situ* calcination method is superior for developing g-C_3N_4 film electrodes for the PEC degradation of organic compounds in water. The calcination temperature has an obvious effect on the PEC activity of the I/g-C_3N_4 film electrode (Fig. 3c). The I/g-C_3N_4 film electrode prepared at a temperature of 500 °C had the highest PEC activity compared to those prepared at other calcination temperatures because of its highest photocurrent response. Although the film electrode prepared at a calcination temperature of 550 °C possessed the highest specific surface area, it did not possess the highest activity. This indicates that the

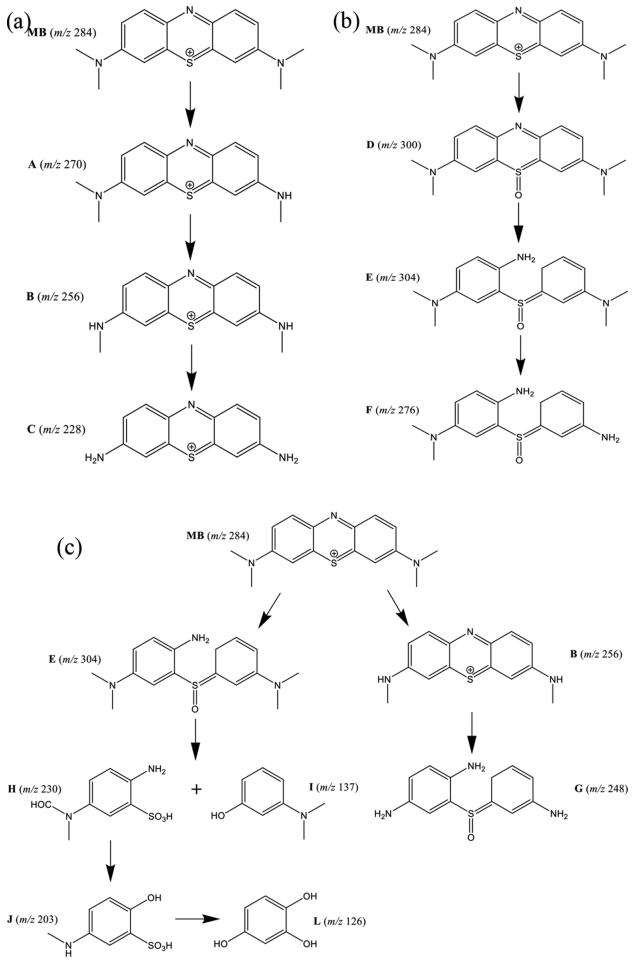

Fig. 4. Degradation pathway of MB in the (a) PC, (b) EC and (c) PEC oxidation systems.

specific surface area is not the determinant factor for the oxidation activity of film electrodes in the PEC reaction.

Fig. 3b shows that the PEC degradation of MB first increased and then decreased when the applied bias increased from 0.5 V to 2 V at a light intensity of 0.96 W/cm^2. The degradation rate of MB peaked at a bias of 1 V, with a removal rate of 62.50%. The degradation effect improved with increasing potential as it enhanced the photogenerated charge carriers and reduced the recombination of electrons and holes. When the bias voltage reached 1 V, the separation of the electrons and holes reached its maximum value, and the space charge layer was close to the film thickness, leading to the best catalytic activity. The degradation rate of MB decreased when the bias potential exceeded 1 V due to the reallocation of the space charge and the Hector Helmholtz layers, reducing the number of photogenerated carriers [27]. Moreover, with increase in the bias potential, the adhesion of g-C_3N_4 film to the ITO glass deteriorated, and some g-C_3N_4 particles could peel off from the electrode and decrease the catalytic activity. This is the main drawback of the I/g-C_3N_4 film electrode. Thus, for successfully conducting the PEC reaction using the I/g-C_3N_4 film electrode, the bias potential should be maintained at a low level.

According to the identified intermediates (Table S3 in Supporting information), the degradation pathways of MB in the PC, EC and PEC reactions are shown in Fig. 4.

Fig. 4a shows the proposed reaction pathway for MB during PC degradation. Firstly, g-C_3N_4 absorbed visible light to produce h^+, and $^{\bullet}OH$ was produced from the reaction between the adsorbed H_2O and h^+. According to a previous study [40], $^{\bullet}OH$ could abstract H from organic compounds, such as paraffin and aromatic hydrocarbons. Therefore, in this study, abstraction of hydrogen from -CH_3 by $^{\bullet}OH$ could lead to the elimination of -CH_3 and the formation of intermediate products such as **A** ($m/z = 270$), **B** ($m/z = 256$), and **C** ($m/z = 228$). No further oxidation products were detected because the concentration of $^{\bullet}OH$ in the system resulted from the high recombination probability of electron-hole pairs in the I/g-C_3N_4 film. This also proved that the g-C_3N_4 film on ITO could not obtain the high degradation efficiency of organic compounds in an aqueous solution.

Compared to that in the literature [41], the MB degradation pathway suggested here involved less intermediates. This suggests that the degradation rate of MB in this study is slower than that reported in the literature. The differences in the degradation rate between them are mainly due to the form of the applied catalyst. We used the g-C_3N_4 film electrode in this study, and the degradation reaction occurred only when the MB molecules diffused to the electrode plate. However, in the literature, the g-C_3N_4 powder was used as the catalyst. The g-C_3N_4 particles could make full contact with the MB molecules.

Fig. 4b shows the reaction pathway for the EC degradation of MB. During the electronic reorganization, sulfhydryl (C−S^+=C) was converted to a sulfoxide (C−(S=O)−C). The intermediate detected by LCMS was **D** ($m/z = 300$). Then **D** to form **E** ($m/z = 304$), because the conversion from C−S^+=C to C−S(=O)−C required the conservation of the double bond conjugation, which resulted in the opening of the central aromatic ring containing both heteroatoms (S and N) [42]. In the EC reaction, the abstraction of hydrogen from −CH_3 by $^{\bullet}OH$ was not observed. This might be attributed to the oxidation effect between the adsorbed $^{\bullet}OH$ on the anode and the produced $^{\bullet}OH$ from the oxidation of water by h^+. Similarly, this degradation path indicated the limited efficiency of EC oxidation using the I/g-C_3N_4 film electrode.

In the PEC degradation of MB (Fig. 4c), there may be two degradation pathways. In the first degradation pathway, the methyl was removed by the active substance with the formation of **B** ($m/z = 256$). Subsequently, the C−S^+=C and C−N=C were attacked and the intermediate **G** ($m/z = 248$) was produced. In the second degradation pathway, the produced $^{\bullet}OH$ directly attacked the C−S^+=C functional group in MB as it had the longest molecular bond with the smallest bond energy in MB; this was revealed by a previous study on the bond length and energy of MB [43]. Thus, the C−S^+=C functional group was prone to being broken, resulting in the formation of the sulfoxide ($m/z = 304$). Additionally, owing to the double bond conjugation, **E** ($m/z = 304$) was broken into **H** ($m/z = 230$) and **I** ($m/z = 137$). The sulfoxide group could undergo a second attack by $^{\bullet}OH$ to produce sulfone and cause the definitive decomposition of the two benzenic rings.

During the PEC reaction, the color of the solution faded over time, and the maximum absorption peak of MB shifted to the direction of a shorter wavelength (blue shift) in the UV–vis spectra (Fig. S8 in Supporting information). This indicates a demethylation reaction in the PEC oxidation process [44]. Therefore, it could be speculated that **H** ($m/z = 230$) could be attacked by $^{\bullet}OH$ to form **J** ($m/z = 203$) and **K** ($m/z = 126$).

Compared to these MB degradation pathways, we observed that the decomposition of MB in the PEC oxidation process was more thorough than that in the PC and EC reactions. This further proved that the I/g-C_3N_4 film electrode could realize the combination of PC and EC oxidation into the PEC oxidation, thereby enhancing the degradation of organic compounds in an aqueous solution [27].

Fig. S10 (Supporting information) shows that the I/g-C_3N_4 film still exhibits high activity for the PEC degradation of MB after being used repeatedly. We inferred that the electrode had good sta-

bility. Additionally, we also conducted experiments with high bias potential and strong light intensity. The shedding of g-C_3N_4 particles was not observed in these experiments. The photographs and SEM images of the fresh and used electrodes showed that the electrode surface changes slightly after the reaction (Fig. S9 in Supporting information). Notably, during the preparation of film electrodes, sonication in water for 1 h did not peel off the g-C_3N_4 films. According to the conclusion in the literature [30], we inferred that the adhesion between g-C_3N_4 and the ITO substrate was strong, and that the g-C_3N_4 film electrode exhibited excellent stability. In the past decades, low efficiency limited the practical application of PC technology, while high energy consumption limited the practical use of EC technology. With the aid of the high quality I/g-C_3N_4 film electrode, which possessed excellent PEC activity and stability, this situation is expected to improve due to the observed synergy between the PC and EC reactions.

In summary, a continuous and uniform g-C_3N_4 film loaded on the ITO glass was prepared by the *in-situ* calcination method. It showed excellent photoelectrocatalysis performance under visible light irradiation for the degradation of MB in water. The removal rate of MB in the PEC reaction was 2.49 and 2.88 times higher than those in the PC and EC reactions. In the PEC reaction, PC and EC degradation could enhance each other, which significantly increased the degradation of MB in water. This resulted in the formation of some monocyclic compounds and more complete degradation. Therefore, our study can promote the environmental application of g-C_3N_4 in water treatment.

Declaration of competing interest

The authors declare that they have no known competing financial interests or personal relationships that could have appeared to influence the work reported in this paper.

Acknowledgment

The authors greatly appreciate the financial support from the National Natural Science Foundation of China (No. 51978658).

Supplementary materials

Supplementary material associated with this article can be found, in the online version, at doi:10.1016/j.cclet.2022.05.049.

References

[1] C.C. Chen, W.H. Ma, J.C. Zhao, Chem. Soc. Rev. 39 (2010) 4206–4219.
[2] C. Kim, S.J. Doh, S.G. Lee, S.J. Lee, H.Y. Kim, Appl. Catal. A: Gen. 330 (2007) 127–133.
[3] J.W. Xinyongguo, Z.S. Shunlizhang, J.F. Zhou, Chin. Chem. Lett. 14 (2003) 419–422.
[4] H.L. Wang, L. Pang, W.F. Jiang, C. Yang, Chin. Chem. Lett. 23 (2012) 1071–1074.
[5] Cao Shaowen, Yu Jiaguo, J. Phys. Chem. Lett. 5 (2014) 2101–2107.
[6] M. Yu, H. Liang, R. Zhan, L. Xu, J. Niu, Chin. Chem. Lett. 32 (2021) 2155–2158.
[7] Y. Xing, X. Wang, S. Hao, X. Zhang, X. Xu, Chin. Chem. Lett. 32 (2021) 13–20.
[8] L. Qian, Z. Ning, Y. Yong, G. Wang, D. Ng, Langmuir 30 (2014) 8965–8972.
[9] H. Xu, H. Zhao, Y. Song, et al., Mater. Sci. Semicond. Process. 39 (2015) 726–734.
[10] Z. Mo, X. Jing, R.L. Zong, Y.F. Zhu, Appl. Catal. B 147 (2014) 229–235.
[11] P. Gibot, F. Schnell, D. Spitzer, Micropor. Mesopor. Mater. 219 (2016) 42–47.
[12] L. Liu, Y. Qi, J. Hu, et al., Mater. Lett. 158 (2015) 278–281.
[13] F. Dong, Z. Zhao, T. Xiong, et al., ACS Appl. Mater. Interfaces 5 (2013) 11392–11401.
[14] C. Liu, X. Dong, Y. Hao, et al., New J. Chem. 41 (2017) 11872–11880.
[15] S.J. Phang, J.M. Goh, L.L. Tan, et al., Environ. Sci. Pollut. Res. 28 (2021) 4388–4403.
[16] T. Li, L. Zhao, Y. He, et al., Appl. Catal. B 129 (2013) 255–263.
[17] X. Zhang, J. Nie, F. Rao, et al., Ceram. Int. 47 (2021) 31302–31310.
[18] Y. Zhang, Z. Chen, J. Li, Z. Lu, X. Wang, J. Energy Chem. 54 (2021) 36–44.
[19] Z. Tong, D. Yang, J. Shi, et al., ACS Appl. Mater. Interfaces 7 (2015) 25693–25701.
[20] P.C. Patra, Y.N. Mohapatra, IEEE J. Electron. Devices 9 (2021) 618–622.
[21] Y. Zhang, Y. Xu, J. Guo, et al., Chem. Eng. J. 420 (2021) 129556.
[22] S. Velmurugan, T.C.K. Yang, ACS Appl. Electron. Mater. 2 (2020) 2845–2856.
[23] S. Kannan, P. Thamaraiselvan, K.A. Rameshkumar, P. Maadeswaran, M. Gomathi, J. Mater. Sci. Mater. Electron. 32 (2021) 18330–18341.
[24] H. Tian, H. Fan, J. Ma, L. Ma, G. Dong, Electrochim. Acta 247 (2017) 787–794.
[25] Y. Xiao, M. Chen, M. Zhang, ChemPhotoChem 3 (2019) 101–106.
[26] W. Liu, Y. Li, F. Liu, et al., Water Res. 151 (2019) 8–19.
[27] F. Liang, Y. Zhu, Appl. Catal. B 180 (2016) 324–329.
[28] S. Yang, X. Feng, X. Wang, K. Muellen, Angew. Chem. Int. Ed. 50 (2011) 5339–5343.
[29] C. Liu, A.Y. Zhang, Y. Si, D.N. Pei, H.Q. Ye, Environ. Sci. Technol. 53 (2019) 7641–7652.
[30] J. Xu, T. Brenner, L. Chabanne, et al., J. Am. Chem. Soc. 136 (2014) 13486–13489.
[31] X. Wang, K. Maeda, A. Thomas, et al., Nat. Mater. 8 (2009) 76–80.
[32] G.M. Veith, L. Baggetto, L.A. Adamczyk, et al., Chem. Mater. 25 (2013) 503–508.
[33] F. Dong, Z. Wang, Y. Li, W.K. Ho, S.C. Lee, Environ. Sci. Technol. 48 (2014) 10345–10353.
[34] Y. Yang, W. Guo, Y. Guo, et al., J. Hazard. Mater. 271 (2014) 150–159.
[35] Y. Zhang, J. Liu, G. Wu, W. Chen, Nanoscale 4 (2012) 5300–5303.
[36] S.C. Yan, Z.S. Li, Z.G. Zou, Langmuir 25 (2009) 10397–10401.
[37] J.G. Yu, K. Wang, Q. Li, et al., Appl. Catal. B 176/177 (2015) 44–52.
[38] S.C. Yan, Z.S. Li, Z.G. Zou, Langmuir 26 (2010) 3894–3901.
[39] G. Wang, J. Zhang, S. Hou, Mater. Res. Bull. 76 (2016) 454–458.
[40] Q. Wang, S. Tian, J. Cun, P. Ning, Desalin Water Treat. 51 (2013) 5821–5830.
[41] Q. Hao, C. Xie, Y. Huang, D. Chen, B.J. Ni, Chin. J. Catal. 41 (2020) 249–258.
[42] A. Houas, H. Lachheb, M. Ksibi, et al., Appl. Catal. B 31 (2001) 145–157.
[43] J.J. Shea, IEEE Electr. Insul. Mag. 20 (2004) 45–45.
[44] T. Zhang, T. Oyama, A. Aoshima, H. Hidaka, N. Serpone, J. Photochem. Photobiol. A 140 (2001) 163–172.